Shape coexistence effects and quasiparticle alignment in ^{81}Sr

E. F. Moore,* P. D. Cottle, C. J. Gross,† D. M. Headly,‡ U. J. Hüttmeier,§ and S. L. Tabor
Department of Physics, Florida State University, Tallahassee, Florida 32306

W. Nazarewicz
Supercomputer Computations Research Institute, Florida State University, Tallahassee, Florida 32306 and Institute of Physics, Warsaw Institute of Technology, PL-00662 Warsaw, Poland

(Received 25 April 1988)

High spin states in ^{81}Sr were investigated in the reactions ^{56}Fe(^{28}Si,2pn) at 103.6 MeV and ^{55}Mn(^{29}Si,$p2n$) at 95.2 MeV using the techniques of in-beam γ-ray spectroscopy. Measurements were made of γ-γ coincidences and γ-ray directional correlations from oriented nuclei. The lifetimes of 12 states and lifetime limits of 10 others were determined with the Doppler shift attenuation method. The data have been analyzed in terms of the Woods-Saxon cranking model. The first crossing observed in the yrast band is attributed to the alignment of a pair of $g_{9/2}$ protons. The irregularities observed in the $J^{(2)}$ moment of inertia in the $K^{\pi}=\frac{5}{2}^{-}$ and $\frac{1}{2}^{(+)}$ bands are interpreted as evidence for the alignment of a $g_{9/2}$ proton pair as well. The coexistence of prolate and oblate configurations at low spin is discussed in terms of the polarization of the soft even-even core by the odd neutron.

I. INTRODUCTION

The neutron deficient nuclei in the $A \approx 80$ region have been found to exhibit varying degrees of collectivity as a function of both particle number and spin. Evidence for the coexistence[1,2] of strongly deformed states with states having near spherical shapes has been seen in the light Ge, Se, and Kr isotopes. Theoretical calculations (see Ref. 3 and references therein) predict similar features in the light Sr and Zr isotopes. The nuclei ^{77}Sr–^{80}Sr have some of the most strongly deformed shapes[4] in this mass region, although in a recent study[5] of ^{80}Sr, evidence of deformation softness was reported. Theoretically, a transition from rotation to vibrationlike excitations is predicted[3] to occur at $N=44$. Experimentally, the $N=44$ nucleus ^{82}Sr has been shown[6] to exhibit behavior typical of a weakly deformed transitional system, having both rotational and vibrational degrees of freedom. Therefore, the odd-mass nucleus ^{81}Sr would be expected to be quite sensitive to the shape polarization effects of quasiparticle excitations on a deformation soft core.

Previously, ^{81}Sr has been studied using both α beams[7] and ^{28}Si beams.[8,9] Arnell *et al.*[7] reported six distinct rotational bands in ^{81}Sr, four of which were studied up to spins of $\frac{15}{2}$ to $\frac{17}{2}$. Lifetime measurements[7] for the lower-lying states in ^{81}Sr implied differing degrees of collectivity for the various bands. In a subsequent study[9] the decay schemes of the yrast and the lowest negative-parity bands were extended to spins of $\frac{33}{2}$ and $\frac{23}{2}$, respectively. Evidence of a crossing in the $g_{9/2}$ yrast band in ^{81}Sr was reported.[9] The present work was initially undertaken to measure the lifetimes of the high spin states reported in Ref. 9 via the Doppler shift attenuation method (DSAM).

Two separate reactions, ^{56}Fe(^{28}Si,2pn)^{81}Sr at 103.6 MeV and ^{55}Mn(^{29}Si,$p2n$)^{81}Sr at 95.2 MeV were used in the DSAM study. The use of a thick free standing Fe target and of a target consisting of a thin layer of Mn evaporated onto a thick Pb foil provided a consistency check for the analysis of the line-shape data because of the different stopping powers. During the data analysis, many new high spin states in ^{81}Sr were identified. Due to the substantial increase in statistical accuracy of the ^{29}Si + ^{55}Mn data over the ^{28}Si + ^{56}Fe data, the construction of the level scheme contained in the present paper was based on data from the ^{55}Mn target.

II. EXPERIMENTAL TECHNIQUES

High spin states in ^{81}Sr were studied using the techniques of γ-ray spectroscopy. The reactions ^{55}Mn(^{29}Si,$p2n$)^{81}Sr and ^{56}Fe(^{28}Si,2pn)^{81}Sr were used at beam energies of 95.2 and 103.6 MeV, respectively. The 95.2 MeV ^{29}Si beam was obtained from the 4.7% abundance in natural Si and accelerated using the Florida State University Tandem-LINAC accelerator facility. The ^{29}Si beam was stripped to a charge state of 8^{+} in the terminal of the tandem and accelerated to 77.4 MeV. This beam was then injected into the superconducting linear accelerator and boosted to 95.2 MeV. Beam currents of about 20 nA on target were thus obtained throughout the duration of the nine day run.

The target for the ^{29}Si beam consisted of a 2 mg/cm^2 layer of natural Mn (100% ^{55}Mn isotopic abundance) evaporated onto a 0.013 cm thick Pb foil. This lead-backed target configuration was chosen in order to provide a stopping medium with a somewhat longer characteristic stopping time than that of the solid Fe target used with the ^{28}Si beam.

In the ^{29}Si + ^{55}Mn experiment, γ-γ coincidences were measured using two Ge detectors with bismuth germanate (BGO) Compton suppression shields and one un-

suppressed Ge(Li) detector. The detectors were arranged such that one of the suppressed Ge detectors was located at an angle of 23° to the beam direction in order to measure Doppler shifted γ-ray line shapes. The other two detectors were located at $\pm 100°$ to the beam direction as a compromise between the minimization of γ-ray Doppler shifting at 90° and coincidences between the back to back 511 keV e^+-e^- annihilation photons.

The coincidence events between all pairs of detectors were recorded on magnetic tape for subsequent off-line analysis. A ^{152}Eu source placed at the target position was used to determine the energy and relative efficiency calibrations for each detector. The γ-γ coincidence events between the two 100° detectors were recalibrated and sorted[10] into a 2500 channel folded triangular matrix in physical memory on a micro VAX-II computer. The coincidences between the 23° detector and either of the two 100° detectors were recalibrated and sorted into an 1800×1800 channel square array in physical memory.

Coincidence spectra were projected from the arrays by setting gates on the γ rays of interest and equal width subtract gates on a suitable nearby region of the spectrum in order to approximately remove background coincidences. Coincidence spectra projected from the 100°-100° array were added to the 100° spectra projected from 23° gates in the 23°-100° array, allowing maximal use of the available statistics.

In the companion study of ^{81}Sr using the reaction ^{56}Fe(^{28}Si,2pn)^{81}Sr, the ^{28}Si beam was stripped to a charge state of 9^+ at the terminal of the tandem and stripped again midway down the high-energy column to a charge state of 12^+ and accelerated to 103.6 MeV. Beam currents of about 5 nA on target were obtained for the four day duration of the run. The target used was a 0.01 cm thick free-standing Fe foil ($\simeq 92\%$ ^{56}Fe abundance).

Two Ge detectors with BGO Compton suppression shields were placed at 0° and 90° to the beam direction. The γ-γ coincidence events were recorded on magnetic tape and subsequently sorted into a square array and projected as described above.

III. THE ^{81}Sr LEVEL SCHEME

The level scheme for ^{81}Sr deduced in the present work is shown in Fig. 1. The results of the present study confirm the low-energy structure for ^{81}Sr reported in Ref. 7. These results also confirm the placement of levels in the $K=\frac{5}{2}^-$ band reported in Ref. 9. There were some discrepancies between the level ordering at the top of the $g_{9/2}$ yrast band as reported in Ref. 9 and those deduced in the present study. The details concerning the level ordering will be discussed below.

Some 20 new γ rays and 15 new levels were identified in ^{81}Sr. The placement of levels in the present study was based on γ-γ coincidence measurements, γ-ray intensity and energy relations, and effective level lifetimes. The assignment of spins was based on the directional correlation of γ rays (DCO ratios) and systematics. The experimental DCO ratio is defined in the present work as

$$R_{\mathrm{DCO}} = \frac{I(\gamma_1 \text{ observed at } \theta_1, \text{ gated by } \gamma_2 \text{ at } \theta_2)}{I(\gamma_1 \text{ observed at } \theta_2, \text{ gated by } \gamma_2 \text{ at } \theta_1)} . \quad (1)$$

All DCO ratios given in Table I have $\theta_1 = 23°$, $\theta_2 = 100°$,

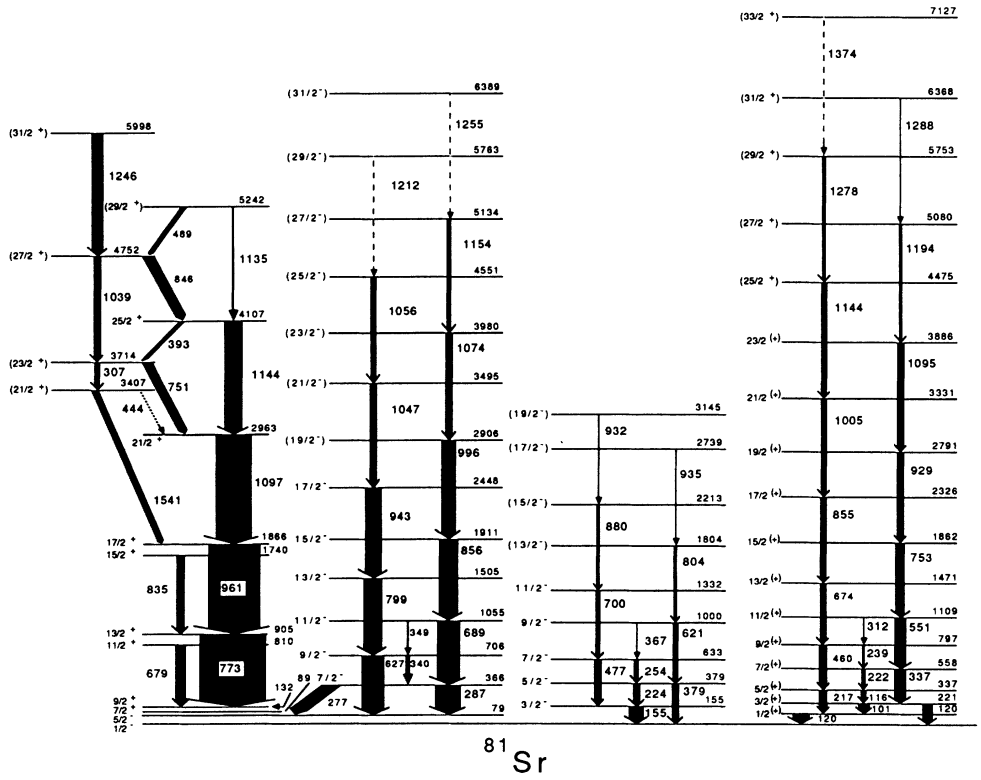

FIG. 1. The level scheme for ^{81}Sr deduced from the present work. Comparison with previous work is discussed in the text.

TABLE I. Energies, intensities, DCO ratios, and multipolarities or $B(E2)/B(M1)$ mixing ratios for transitions in ^{81}Sr. Errors in the last digits are shown in parentheses.

E_{lev} (keV)	E_γ (keV)	$I_i \rightarrow I_f$	A_0[a]	R_{DCO}	δ or Mult.
810	679	$\frac{11}{2} \rightarrow \frac{9}{2}$	16.7(17)		$M1/E2$[c]
905	773	$\frac{13}{2} \rightarrow \frac{9}{2}$	121.9(15)	1.23(3)	$E2$
1740	835	$\frac{15}{2} \rightarrow \frac{13}{2}$	12.0(14)	0.30(7)	$M1/E2$
1866	961	$\frac{17}{2} \rightarrow \frac{13}{2}$	100.0(20)	1.02(1)	$E2$
2963	1097	$\frac{21}{2} \rightarrow \frac{17}{2}$	70.3(35)	1.01(3)	$E2$
3407	1541	$(\frac{21}{2}') \rightarrow \frac{17}{2}$	18.3(42)	1.22(35)	$E2$
3714	307	$(\frac{23}{2}) \rightarrow (\frac{21}{2}')$	4.8(12)	0.70(17)	$M1/E2$
	751	$(\frac{23}{2}) \rightarrow \frac{21}{2}$	18.9(38)	0.23(8)	0.3(1)[b]
4107	393	$\frac{25}{2} \rightarrow (\frac{23}{2})$	3.8(10)	0.42(12)	$M1/E2$
	1144	$\frac{25}{2} \rightarrow \frac{21}{2}$	36.3(54)	1.04(18)	$E2$
4752	646	$(\frac{27}{2}) \rightarrow \frac{25}{2}$	17.2(43)	0.38(9)	0.1(1)[b]
	1039	$(\frac{27}{2}) \rightarrow (\frac{23}{2})$	10.9(21)	1.15(33)	$E2$
5242	489	$(\frac{29}{2}) \rightarrow (\frac{27}{2})$	7.5(30)	0.51(13)	$M1/E2$
	1135	$(\frac{29}{2}) \rightarrow \frac{25}{2}$	<2		$E2$
5998	1246	$(\frac{31}{2}) \rightarrow (\frac{27}{2})$	20.3(45)	1.16(38)	$E2$
366	277	$\frac{7}{2} \rightarrow \frac{7}{2}$	26.5(26)		$E1$[c]
	287	$\frac{7}{2} \rightarrow \frac{5}{2}$	47.4(23)		$M1/E2$[c]
706	340	$\frac{9}{2} \rightarrow \frac{7}{2}$	1.5(5)		$M1/E2$
	627	$\frac{9}{2} \rightarrow \frac{5}{2}$	39.9(22)		$E2$
1055	349	$\frac{11}{2} \rightarrow \frac{9}{2}$	<1	0.80(15)	$M1/E2$
	689	$\frac{11}{2} \rightarrow \frac{7}{2}$	41.2(21)		$E2$
1505	799	$\frac{13}{2} \rightarrow \frac{9}{2}$	38.3(28)	1.10(8)	$E2$
1911	856	$\frac{15}{2} \rightarrow \frac{11}{2}$	30.5(40)	0.97(12)	$E2$
2448	943	$\frac{17}{2} \rightarrow \frac{13}{2}$	30.7(38)	1.21(26)	$E2$
2906	996	$(\frac{19}{2}) \rightarrow \frac{15}{2}$	25.5(46)	1.22(30)	$E2$
3495	1047	$(\frac{21}{2}) \rightarrow \frac{17}{2}$	16(7)		$E2$
3980	1074	$(\frac{23}{2}) \rightarrow (\frac{19}{2})$	11.7(36)	1.33(32)	$E2$
4551	1056	$(\frac{23}{2}) \rightarrow (\frac{21}{1})$	10(6)		$E2$
5134	1154	$(\frac{27}{2}) \rightarrow (\frac{23}{2})$	6.0(25)		$E2$[d]
155	155	$\frac{3}{2} \rightarrow \frac{1}{2}$	16.2(20)		$M1/E2$[c]
379	224	$\frac{5}{2} \rightarrow \frac{3}{2}$	12.0(15)		$M1/E2$[c]
	379	$\frac{5}{2} \rightarrow \frac{1}{2}$	11.6(23)		$E2$[c]
633	254	$\frac{7}{2} \rightarrow \frac{5}{2}$	4.6(13)		$M1/E2$[c]
	477	$\frac{7}{2} \rightarrow \frac{3}{2}$	14.4(22)		$E2$[c]
1000	367	$\frac{9}{2} \rightarrow \frac{7}{2}$	<1		$M1/E2$[c]
	621	$\frac{9}{2} \rightarrow \frac{5}{2}$	7.3(16)		$E2$[c]
1332	700	$\frac{11}{2} \rightarrow \frac{7}{2}$	8.5(20)		$E2$[c]
1804	804	$(\frac{13}{2}) \rightarrow \frac{9}{2}$	3.9(18)		$E2$[c]
2213	880	$(\frac{15}{2}) \rightarrow \frac{11}{2}$	6.9(24)		$E2$[c]
2739	935	$(\frac{17}{2}) \rightarrow (\frac{13}{2})$	<2		$(E2)$[d]
3145	932	$(\frac{19}{2}) \rightarrow (\frac{15}{2})$	<1		$(E2)$[d]
120	120	$\frac{1}{2} \rightarrow \frac{1}{2}$	32.8(21)		$E1$[c]
221	101	$\frac{3}{2} \rightarrow \frac{1}{2}$	16.4(17)	0.84(15)	$M1/E2$
	221	$\frac{3}{2} \rightarrow \frac{1}{2}$	20.5(15)		$E1$[c]

TABLE I. (*Continued*).

E_{lev} (keV)	E_γ (keV)	$I_i \rightarrow I_f$	A_0[a]	R_{DCO}	δ or Mult.
337	116	$\frac{5}{2} \rightarrow \frac{3}{2}$	9.0(12)	0.40(7)	$M1/E2$
	217	$\frac{5}{2} \rightarrow \frac{1}{2}$	18.0(18)		$E2$[c]
558	222	$\frac{7}{2} \rightarrow \frac{5}{2}$	3.4(7)		$M1/E2$[c]
	337	$\frac{7}{2} \rightarrow \frac{3}{2}$	23.5(20)		$E2$[c]
797	239	$\frac{9}{2} \rightarrow \frac{7}{2}$	2.9(5)	0.55(8)	$M1/E2$
	460	$\frac{9}{2} \rightarrow \frac{5}{2}$	17.2(15)		$E2$[c]
1109	312	$\frac{11}{2} \rightarrow \frac{9}{2}$	<1	0.75(10)	$M1/E2$
	551	$\frac{11}{2} \rightarrow \frac{7}{2}$	24.2(18)	1.05(3)	$E2$
1471	674	$\frac{13}{2} \rightarrow \frac{9}{2}$	16.5(17)	1.03(6)	$E2$
1862	753	$\frac{15}{2} \rightarrow \frac{11}{2}$	22.1(21)	1.17(12)	$E2$
2326	855	$\frac{17}{2} \rightarrow \frac{13}{2}$	14.5(18)	1.09(16)	$E2$
2791	929	$\frac{19}{2} \rightarrow \frac{15}{2}$	18.7(20)	1.04(17)	$E2$
3331	1005	$\frac{21}{2} \rightarrow \frac{17}{2}$	12.6(16)	1.07(20)	$E2$
3886	1095	$\frac{23}{2} \rightarrow \frac{19}{2}$	13.3(21)	1.29(28)	$E2$
4475	1144	$(\frac{25}{2}) \rightarrow \frac{21}{2}$	7.6(25)	1.40(35)	$E2$
5080	1194	$(\frac{27}{2}) \rightarrow \frac{23}{2}$	6.7(28)	1.8(5)	$E2$
5753	1278	$(\frac{29}{2}) \rightarrow (\frac{25}{2})$	5.3(32)		$E2$[d]
6368	1288	$(\frac{31}{2}) \rightarrow (\frac{27}{2})$	<2		$E2$[d]

[a]Relative intensity normalized to the 961 keV transition.
[b]Obtained from a reanalysis of data taken in Ref. 9.
[c]Reference 7.
[d]Based on systematics.

and the gate transition is of known $E2$ multipolarity. The DCO ratios for pure $E2$ transitions are expected to be unity; whereas, if γ_1 is of dipole multipolarity then the DCO ratio will vary from $\simeq 0$ to $\simeq 2$, depending on the mixing ratio of γ_1 and the degree of nuclear alignment.[11] Table I summarizes the results of the γ-ray energy, intensity, DCO ratio measurements, and the multipolarities or mixing ratios for transitions in ^{81}Sr. The details of the experimental results concerning each band in ^{81}Sr will be discussed below.

A. The $g_{9/2}$ yrast band

The bandhead of the yrast band in ^{81}Sr was reported[7] to be the $\frac{9}{2}^+$ level at 132 keV. A cascade of $E2$ transitions was observed up to the 2961 keV level. At about the same time, this band was studied[8] up to the $\frac{25}{2}^+$ level at 4107 keV. In a subsequent study,[9] Hicks *et al.* extended this band up to spin $\frac{33}{2}$. The yrast band in ^{81}Sr was reported to consist of stretched $E2$ transitions up to spin $\frac{29}{2}$, above which two $M1/E2$ mixed transitions with energies of 646 and 751 keV were placed.

The 100° summed spectrum gated on the 773, 961, and 1097 keV transitions in the yrast band is shown in Fig. 2. All γ rays previously assigned to this band are present in this spectrum, as are several new γ rays. The results of the present study confirm the level placements reported for the yrast band in Refs. 7 and 8. The present data are also consistent with the level placement reported in Ref.

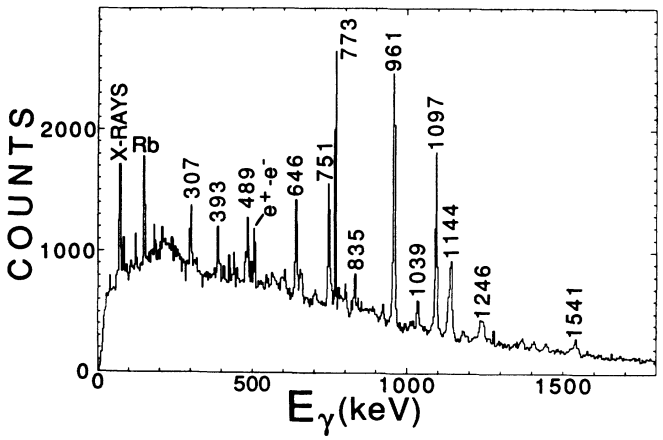

FIG. 2. The spectrum of γ rays observed at 100° in coincidence with the 773, 961, and 1097 keV transitions in the yrast band of ^{81}Sr. The γ rays in ^{81}Sr are labeled by their energies in keV.

9 up to the $\frac{21}{2}^+$ level at 2963 keV, and the placement of the 1144 keV transition. Figure 3 shows the 100° spectra in coincidence with the 646 keV [Fig. 3(a)] and the 751 keV [Fig. 3(b)] transitions. Clearly, the 1144 keV transition is not in coincidence with the 751 keV γ ray. These results contradict the placement of the 751 keV transition as reported in Ref. 9. The authors reported that limited statistical accuracy did not allow a reliable gate to be set on the 751 keV transition in order to prove coincidences with the higher-lying members of the yrast band.

The presence of a 393 keV γ ray, with a DCO ratio consistent with dipole multipolarity, in coincidence with the 751 keV γ ray and not in coincidence with the 1144 keV transition, strongly supports the placement of the 751 keV transition as shown in Fig. 1. The mixed dipole character of both the 393 and 751 keV γ rays makes $\frac{23}{2}$ the most likely spin for the 3714 keV level. A 1039 keV γ ray was seen in coincidence with the 751 keV transition [Fig. 3(b)], as well as with lower-lying transitions in the yrast band (Fig. 2). The presence of this γ ray and the fact that the sum of the 393 and 646 keV γ ray energies is equal to 1039 keV suggests that the 646 keV transition feeds directly into the $\frac{25}{2}^+$ level at 4107 keV. Since the 646 keV γ ray is a mixed $M1/E2$ transition[9] and the 1039 keV γ ray has a DCO ratio consistent with stretched $E2$ multipolarity, the spin of the 4752 keV level is most probably $\frac{27}{2}$.

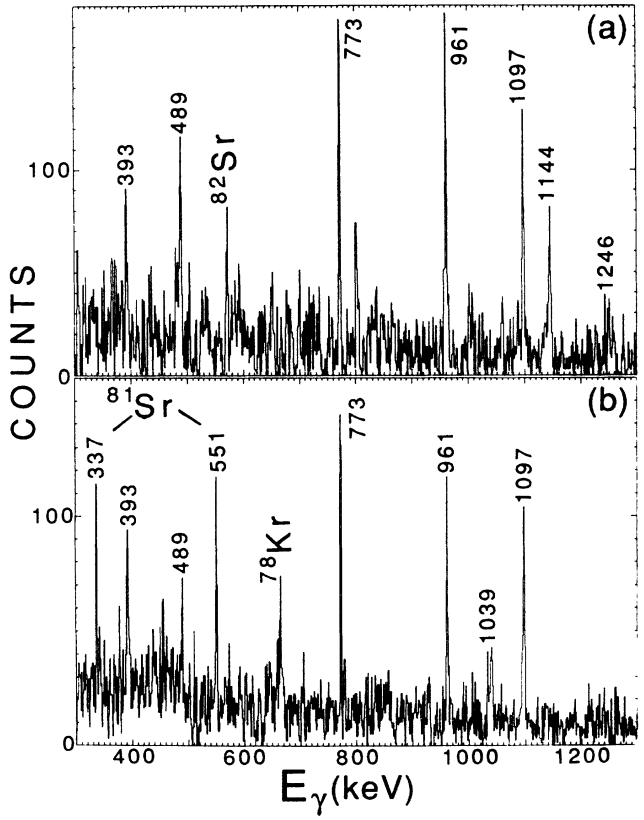

FIG. 3. The spectra of γ rays observed at 100° in coincidence with the (a) 646 keV and (b) 751 keV transitions. The 337 and 551 keV γ rays seen in (b) result from an overlap of the gate with the 753 keV transition in the $K^\pi = \frac{1}{2}^{(+)}$ band in ^{81}Sr.

The γ-γ coincidences and γ-ray intensity relations indicate that the 1246 keV transition feeds directly into the $\frac{27}{2}^+$ state at 4752 keV. A 489 keV γ ray was seen in coincidence with the lower-lying transitions in the ^{81}Sr yrast band (see Figs. 2 and 3). The γ-ray intensity relations suggest that this transition lies above the 4752 keV level. The DCO ratio for the 489 keV γ ray is consistent with $\Delta I = 1$, leading to a tentative spin assignment of $(\frac{29}{2}^+)$ for the 5242 keV level. A rather weak 1135 keV γ ray was seen in coincidence with the 1144 keV transition. The spectrum gated on a narrow region around 1135 keV clearly shows coincidences with the lower-lying transitions in the ^{81}Sr yrast band (see Fig. 4). This evidence gives an additional confirmation of the placement of a level at 5242 keV in this band. Although there were several candidates for even higher-lying transitions in the yrast band, no definite placements could be made.

A relatively strong 1541 keV γ ray was seen in coincidence with the 773 and 961 keV transitions in the yrast cascade in ^{81}Sr. A 307 keV γ ray was also seen in coincidence with these transitions, as well as with the 1541 keV γ ray. The DCO ratios for these new γ rays indicate $E2$ and $M1/E2$ multipolarities for the 1541 and 307 keV transitions, respectively. The γ-ray intensity relations suggest the placement of the 307 keV γ ray above the 1541 keV transition. From the multipolarities of these γ rays, a tentative spin assignment of $\frac{21}{2}$ has been made for the 3407 keV level.

The multipole mixing ratios for the 646 and 751 keV γ rays were obtained from a reanalysis of the angular distribution data of Hicks *et al.*[9] using the method suggested in Ref. 12. A Gaussian shape was assumed for the distribution of magnetic substates. It has been shown[12] that the theoretical angular distributions are rather insensitive to variations in the width σ of the substate distribution for $0 \leq \sigma \leq 2$. Figure 5 shows the χ^2 curve as a function of the arctangent of the mixing ratio δ for both the 646 and 751 keV γ rays. The best fit mixing ratios for these transitions are given in Table I. A second minimum appears in the χ^2 curve for the 646 keV transition corresponding to a mixing ratio value of about $\delta \simeq 5$. By using

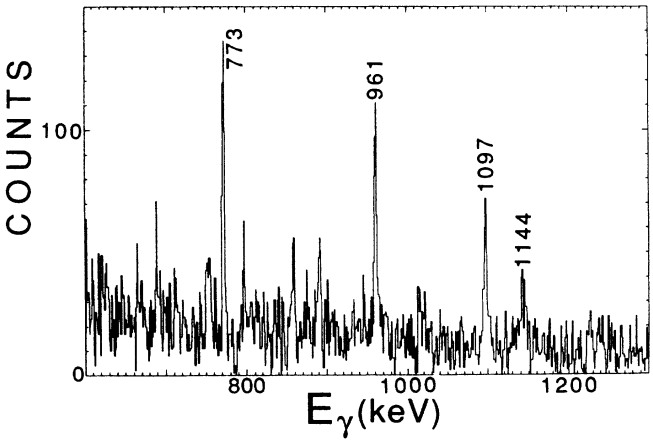

FIG. 4. The spectrum of γ rays observed at 100° in coincidence with the 1135 keV transition.

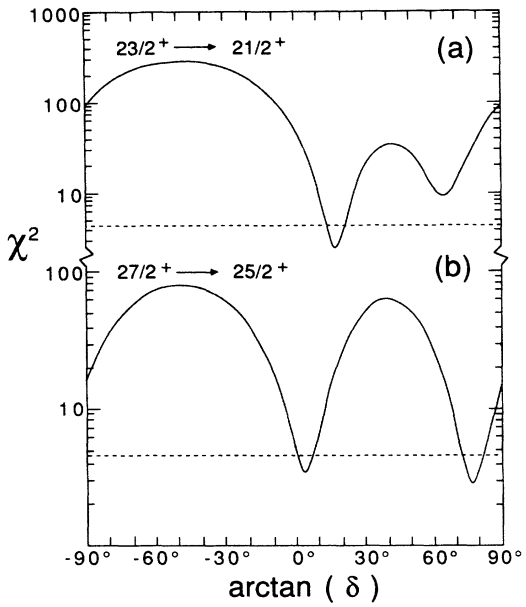

FIG. 5. The goodness-of-fit χ^2 as a function of the $E2/M1$ mixing ratio δ for the angular distributions (Ref. 9) of the (a) 646 keV and (b) 751 keV γ rays. The dashed line indicates the 0.1% confidence limit.

the mean lifetime measured for the 646 keV transition (see Sec. IV) and this mixing ratio value, an $E2$ strength of about 590 single particle units is obtained for the 646 keV γ ray. This $B(E2)$ value is inconsistent with the $B(E2)$ values for other transitions in this band and is unreasonably large, allowing the rejection of the larger mixing ratio value. Using the mixing ratios shown in Table I and the lifetimes measured for the 646 and the 751 keV transitions, $B(M1)$ values of 0.37 $(+0.14/-0.09)$ and 0.17 $(+0.12/-0.05)$ μ_N^2, respectively, were obtained for these transitions.

B. The $K^\pi = \frac{5}{2}^-$ band

Arnell *et al.*[7] reported a negative-parity band based on the $\frac{5}{2}^-$ state at 79 keV up to a tentative spin of $\frac{17}{2}^-$. This band was extended up to $\frac{23}{2}^-$ in Ref. 9, with a possible 1056 keV transition from a $\frac{25}{2}^-$ state. The results of the present study are in complete agreement with the previously reported level placements in the $K^\pi = \frac{5}{2}^-$ band. The existence of the 1056 keV transition and the $\frac{25}{2}^-$ state reported in Ref. 9 was also verified. Figure 6 shows the 100° coincidence spectra for both cascades in the $K^\pi = \frac{5}{2}^-$ band. An 1154 keV γ ray was seen in coincidence with the 277, 287, 689, 996, and 1074 keV cascade of transitions. Intensity relations indicate that this transition feeds directly into the $\frac{23}{2}^-$ level at 3980 keV. The DCO ratio for the 1154 keV γ ray is consistent with $E2$ multipolarity, leading to a spin assignment of $\frac{27}{2}^-$ for the 5134 keV level.

The data also indicate peaks at 1212 and 1255 keV are in coincidence with transitions in the (627, 799, 943, 1047, and 1056 keV) and the (277, 287, 689, 996, 1074, and 1154 keV) cascades, respectively (see Fig. 6). Due to limited statistical accuracy and difficulty in setting reliable gates on these two γ rays, it was not possible to verify their presence in the respective cascades. Therefore, these transitions and the corresponding levels have been drawn as dashed lines in Fig. 1.

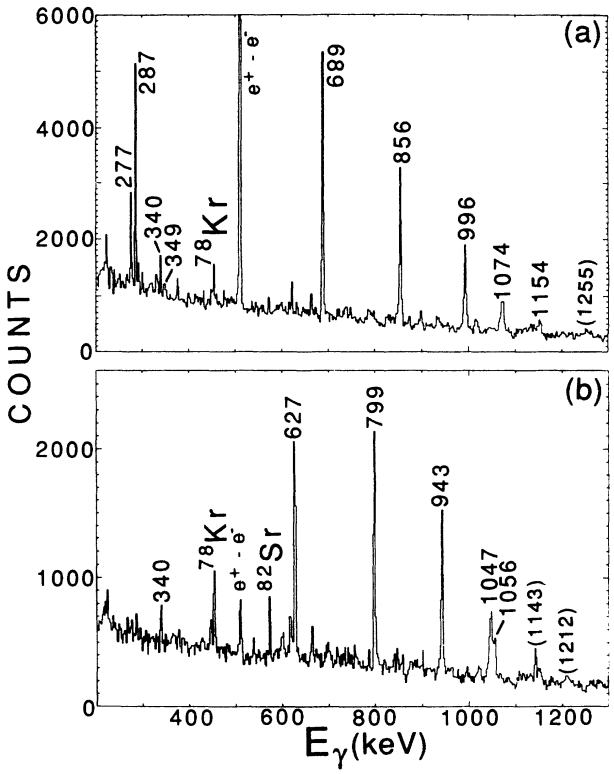

FIG. 6. The spectra of γ rays observed at 100° in coincidence with (a) the 277, 287, 689, 856, 996, and 1074 keV transitions in the $\alpha = -\frac{1}{2}$, $K^\pi = \frac{5}{2}^-$ band and with (b) the 627, 799, 943, 1047, and 1056 keV transitions in the $\alpha = +\frac{1}{2}$, $K^\pi = \frac{5}{2}^-$ band.

Neither Ref. 7 nor Ref. 9 report the presence of $M1$ transitions between the members of this band. In the present study, 340 and 349 keV γ rays were seen in coincidence with transitions belonging to this band. The DCO ratios for the two γ rays are consistent with dipole multipolarity, supporting the placement shown in Fig. 1.

An 1143 keV γ ray was seen in coincidence with the 627, 799, and 943 keV transitions. The forward angle spectra showed virtually no Doppler shift for this γ ray, indicating a relatively long effective lifetime compared to the members of the rotational cascade. Due to the relatively weak intensity of this γ ray, it was not possible to set a reliable gate. Therefore, this γ ray was not placed in the decay scheme shown in Fig. 1.

C. The $K^\pi = \frac{1}{2}^-$ band

The $K^\pi = \frac{1}{2}^-$ band reported in Ref. 7 was populated relatively weakly in the present study. All transitions previously placed[7] in this band were seen and their placement was confirmed. Figure 7 shows the 100° coincidence spectrum gated on transitions in both cascades belonging to this band. New γ rays were seen in coincidence with members of each cascade. The γ-ray inten-

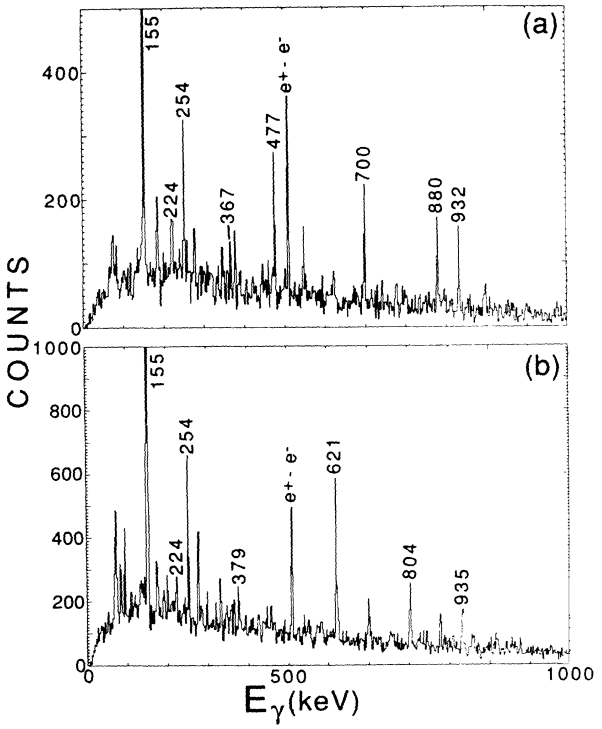

FIG. 7. The spectra of γ rays observed at 100° in coincidence with (a) the 477, 700, and 880 keV transitions in the $\alpha=-\frac{1}{2}$, $K^\pi=\frac{1}{2}^-$ band and with (b) the 224, 378, and 804 keV transitions in the $\alpha=+\frac{1}{2}$, $K^\pi=\frac{1}{2}^-$ band.

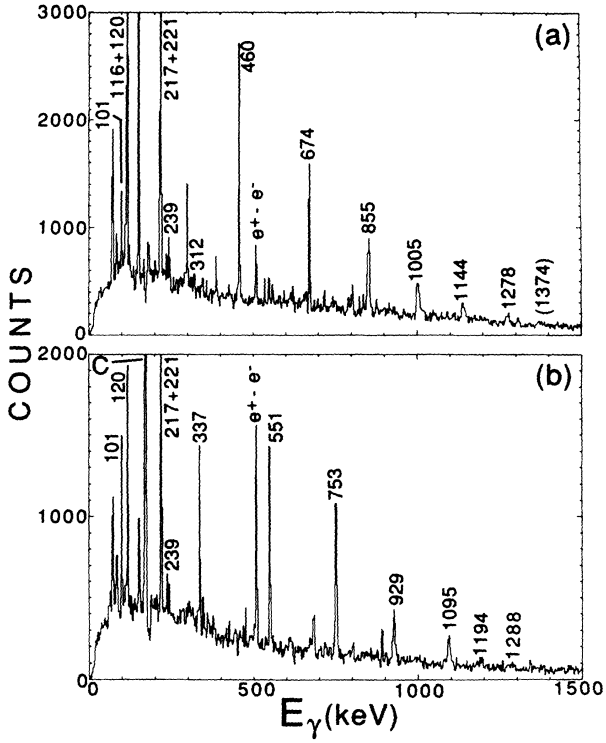

FIG. 8. The spectra of γ rays observed at 100° in coincidence with (a) the 116, 217, 460, and 674 keV transitions in the $\alpha=+\frac{1}{2}$, $K^\pi=\frac{1}{2}^{(+)}$ band and with (b) the 337 and 551 keV transitions in the $\alpha=-\frac{1}{2}$, $K^\pi=\frac{1}{2}^{(+)}$ band.

sity relations support the placement of the 932 and 935 keV γ rays at the top of the (477, 700, and 880 keV) and the (379, 621, and 804 keV) cascades, respectively. Due to the relatively weak intensities of these γ rays, it was not possible to determine their DCO ratios. Therefore, the tentative spin assignments for the 2739 and 3145 keV levels are based on systematics.

D. The $K^\pi=\frac{1}{2}^{(+)}$ band

A fourth rotational band in ^{81}Sr was reported in Ref. 7. This band was shown[7] to be based on a level at 120 keV having a spin of $\frac{1}{2}$. Using arguments based on angular distribution polarization and lifetime measurements, Arnell *et al.*[7] tentatively assigned positive parity to the 120 and 221 keV levels in this band. States in this band were observed up to spin $\frac{17}{2}$.

In the present study, seven new levels and nine new γ rays were placed in the decay scheme for this band. Figure 8 shows the 100° spectra gated on transitions in this band. The placement of levels reported in Ref. 7 was confirmed. The DCO ratios for the 239 and 312 keV γ rays are consistent with $M1/E2$ multipolarity. All of the other new γ rays whose DCO ratios were measured were consistent with stretched quadrupole multipolarity. There appears to be a peak at 1374 keV in coincidence with transitions in the (217, 460, 674, 855, 1005, 1144, and 1278 keV) cascade. Since it was not possible to set a reliable gate around this peak, the 1374 keV transition and the corresponding level have been drawn as dashed lines in Fig. 1.

IV. ANALYSIS OF LIFETIMES DATA

The lifetimes of high spin states in ^{81}Sr were obtained from an analysis of the Doppler shifted line shapes measured at forward angles to the beam direction. In order to check the consistency of the Doppler-shift attenuation method analysis, line-shape data from both the ^{28}Si + ^{56}Fe and the ^{29}Si + ^{55}Mn reactions were used. Background subtracted coincidence spectra gated on transitions lying below the transition of interest were added together to improve statistical accuracy for each set of data. A computer code was developed to perform the DSAM analysis. Doppler shifted line shapes are calculated for a range of lifetime values. The detector response is folded into the theoretical line shapes, which are then compared to the experimental data. The lifetime value giving the best fit to the experimental line shape is then taken to be the lifetime of the state of interest. The details concerning the line-shape fitting process are described below.

A. Stopping powers

In the simulation of the recoil slowing down process, the stopping power was separated into an electronic and a nuclear component. The tabulated values[13] for the electronic stopping powers were scaled[14] to the experimental stopping powers[15] for He:

$$(dE/dx)_e = dE^{(N-S)}/dx\,(dE_\alpha^{(Z-C)}/dx)/(dE_\alpha^{(N-S)}/dx)\ , \tag{2}$$

where the superscript $N-S$ represents the tabulated values of Ref. 13, and $Z-C$ the experimental values of Ref. 15.

The nuclear component of the stopping powers was calculated using the well-known Bohr ansatz[16]

$$(d\epsilon/d\rho)_n = \frac{1}{2\epsilon}\ln(2\epsilon) \tag{3}$$

where ϵ and ρ are the reduced energy and range units,[17] respectively. Due to the relatively high initial recoil velocities ($\beta \simeq 0.03$) in both reactions, the nuclear stopping power has only a minor effect on the quality of the fit. The angular straggling of the ^{81}Sr ions due to atomic collisions was treated in Blaugrund's approximation.[18]

B. Kinematics

In the line-shape calculations for each set of data, the target was divided into several imaginary layers. Theoretical line shapes, calculated for nuclei produced in each layer and recoiling through the remainder of the target or backing, were combined for the entire target. The projectile velocity as a function of target depth was calculated by interpolating the stopping powers[13] for the beam ions in the target material. The production of residual nuclei in each target layer was weighted by the relative cross section at the average beam energy in that layer. For the ^{28}Si + ^{56}Fe reaction, the experimentally measured ^{81}Sr production cross section[19] was used. For the ^{29}Si + ^{55}Mn reaction, the cross section calculated with the statistical model code PACE2 (Ref. 20) was used.

The recoil velocity for the ^{81}Sr ions produced in each target layer was calculated from simple kinematics. The distribution of recoil velocities due to the evaporation of light particles (assumed to be isotropic in the center-of-mass frame) was assumed to have a Gaussian shape. The width of the distribution was estimated to be about 10% based on the proton and neutron evaporation spectra obtained from PACE2 calculations. The finite solid angle subtended by the γ-ray detector was also included in the analysis.

C. Corrections for delayed feeding

The influence of delays due to both direct and cascade feeding was treated in the analysis. The population of the state of interest from cascade feeding was determined from γ-γ coincidence measurements. The experimentally determined lifetimes of the transitions feeding the state of interest were then used to correct for cascade feeding delays. Therefore, the analysis started with the highest-lying observed transition in a given band and proceeded in an iterative fashion down the cascade. The lifetime value obtained for a given transition with no cascade feeding correction is referred to as the effective lifetime and represents the composite lifetime of the state of interest and all of the transitions feeding it. The effective lifetimes thus give a very good indication of the relative ordering of transitions in a given cascade.

The continuum feeding times were estimated to be about 0.1 ps for the highest-lying transitions, increasing by about 0.03 ps per MeV of deexcitation. This assumption is consistent with the side feeding times used in several recent studies[21–23] of nuclei in the mass 80 region performed with heavy-ion reactions. In other recent studies[5,24] continuum feeding times somewhat longer than those used in the present work have been reported in other $A \simeq 80$ nuclei. In ^{80}Sr, side feeding times equal to the effective lifetime of the preceding transition were reported.[5] It is likely that the side feeding time varies for different nuclei and different reaction mechanisms.

The use of longer continuum feeding times did not significantly affect the quality of the fits to the present line-shape data. The longer feeding times did, however, result in shorter best fit lifetimes for the states of interest. The continuum feeding times assumed in the present study probably represent a lower limit to the actual feeding times. Since the same prescription was used for the side feeding times for all of the lifetimes measured in the present study, longer feeding times would result in shorter lifetimes for the states in each band. Thus, the relative differences in the transition rates between the bands in ^{81}Sr would not be significantly affected.

D. Results of lifetime measurements

The results of the present DSAM lifetime measurements are presented in Table II. Typical line-shape fits from both sets of data are shown in Fig. 9. Lifetime values obtained from both the ^{28}Si + ^{56}Fe and the ^{29}Si + ^{55}Mn data are given, where available. Due to limited statistical accuracy, it was not possible to extract lifetimes from the ^{28}Si + ^{56}Fe data for the $K^\pi = \frac{1}{2}^{(+)}$ band. The adopted lifetimes shown in Table II were obtained from a weighted average of the lifetime values determined from both sets of data, with the exception of those for the $K^\pi = \frac{1}{2}^{(+)}$ band. The error bars for each set of data include both statistical error and an estimated 20% uncertainty in the stopping powers.

The mean lifetimes and transition strengths determined in the present study and those measured previously[7] are included in Table II. Table II also presents the transition quadrupole moments $|Q_t|$, as determined from the mean lifetimes of the stretched $E2$ transitions in ^{81}Sr. The Q_t values were calculated from the simple rotational formula

$$B(E2, I \rightarrow I-2) = 5/16\pi \langle IK20 \mid I-2K \rangle^2 Q_t^2\ , \tag{4}$$

where K is the bandhead spin. A value of $K = \frac{5}{2}$ was assumed for the $g_{9/2}$ yrast band.

V. ONE-QUASI-NEUTRON BANDHEADS IN ^{81}Sr

In contrast to the other odd-mass nuclei from the $A \simeq 80$ region, the low-energy part of the level scheme of ^{81}Sr has been identified in detail. In Ref. 7 six rotational bands built on one-quasi-neutron excitations have been found. This rich structure offers a unique possibility to test theoretical predictions about various neutron excitations around $N=43$.

Shape properties of the even-even cores of ^{81}Sr have been recently discussed in Sec. IV of Ref. 3 devoted to ^{83}Zr, the neighboring $N=43$ isotone. It is expected that the transition from a well-deformed rotationlike regime to a deformation-soft vibrationlike pattern is expected to take place at $N=44$. The $N=42$ core, ^{80}Sr, is calculated to be well deformed in its ground state, $\beta_2=0.38$, but an oblate-shaped minimum $\beta_2=0.2$ ($\gamma=-60°$) is also predicted by the calculations. ^{82}Sr ($N=44$) is predicted to be nearly spherical in its ground state, with an excited well-deformed prolate minimum. One can thus expect that in ^{81}Sr different quasiparticle excitations would polarize the nuclear shape towards different regions in the (β_2,γ) plane depending on their intrinsic quadrupole moment, intrinsic angular momentum, and distance from the Fermi surface.

The ground state of ^{81}Sr is an $I^{\pi}=\frac{1}{2}^-$ state, as in the other $N=43$ isotones: ^{75}Ge, ^{77}Se, ^{79}Kr, and ^{83}Zr. The bandhead calculations of Ref. 25 based on the deformed Woods-Saxon average potential indicate that this level can be associated with $[301]\frac{1}{2}$ orbital. The predicted quadrupole deformation for this state is rather large, $\beta_2=0.29$. A $\frac{5}{2}^-$ bandhead is seen at a low excitation energy of 79 keV. The only negative-parity $K=\frac{5}{2}$ Nilsson orbital around $N=43$ is the $[303]\frac{5}{2}$ level originating from

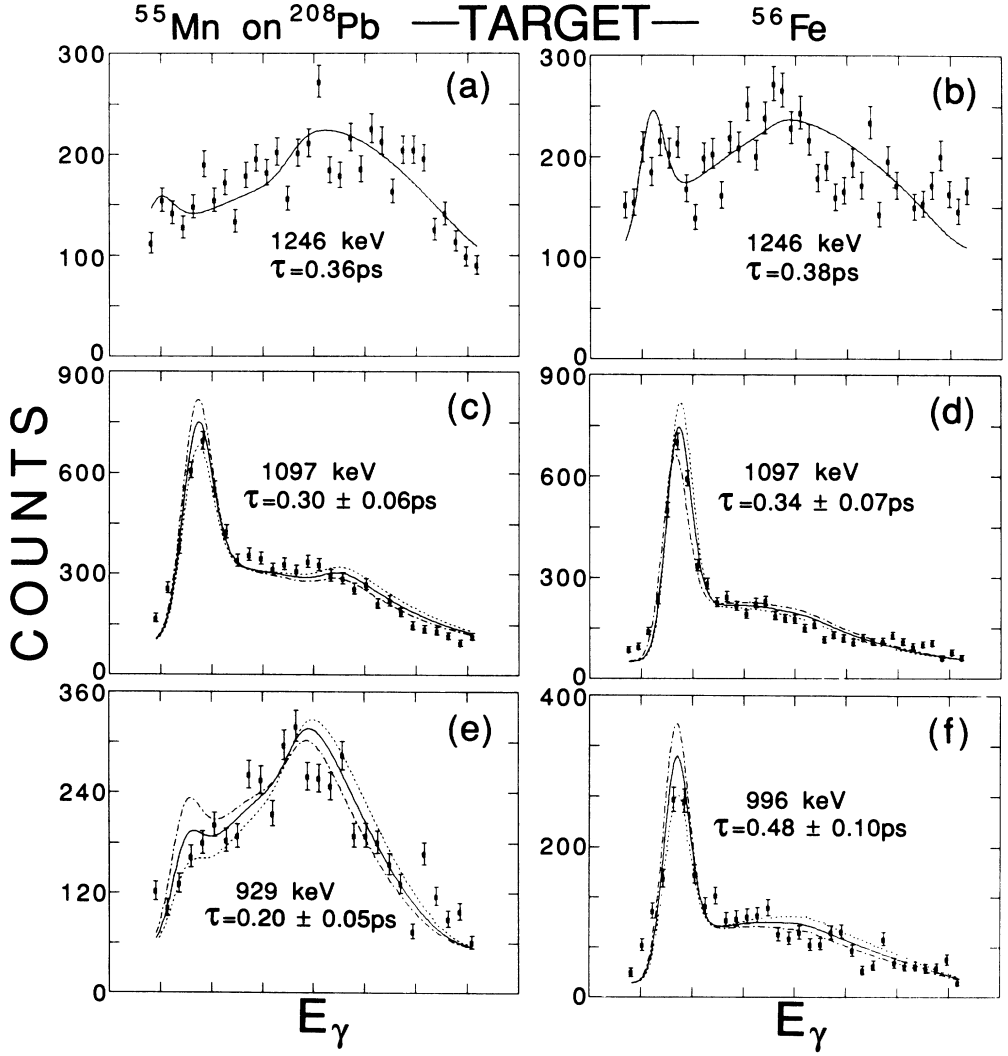

FIG. 9. Examples of DSAM fits to the forward angle coincidence γ spectra. The spectra on the left were measured with the ^{29}Si + ^{55}Mn reaction which used a thin ^{55}Mn target evaporated onto a Pb backing. Those on the right were measured with the ^{28}Si + ^{56}Fe reaction which used a thick ^{56}Fe target.

the $f_{5/2}$ subshell. The calculated equilibrium deformation of this state is $\beta_2=0.28$. The third low-lying negative-parity state predicted theoretically is the $[301]\frac{3}{2}$ orbital. According to the calculations it polarizes the core towards a large prolate deformation of $\beta_2=0.35$. Experimentally, the best candidate for this excitation is a 295 keV $I^\pi=\frac{3}{2}^-$ state observed in Ref. 7.

It is interesting to note that the $[303]\frac{5}{2}$ and $[301]\frac{3}{2}$ states form a pseudospin doublet[26,27] with $[\tilde{N}\,\tilde{n}_z\tilde{\Lambda}]=[\tilde{2}\,\tilde{0}\,\tilde{2}]$. In the limit of the pseudo-SU(3) symmetry[28] this doublet, together with the $[301]\frac{1}{2}$ level (which corresponds to the pseudo-orbital assignment $[\tilde{2}\,\tilde{0}\,\tilde{0}]$), constitute a complete pseudo-oscillator subshell $\tilde{N}=2$, $\tilde{n}_z=0$ with the orbital $\tilde{N}-\tilde{n}_z+1=3$ degeneracy. It has recently been shown[29] that the pseudo-SU(3) symmetry is fairly well obeyed by a realistic average field.

TABLE II. The results of the lifetime measurements.

$E_{\rm lev}$ (keV)	I_i^π	E_γ (keV)	$\tau^{\rm a}$ (ps)	$\tau^{\rm b}$ (ps)	$\tau^{\rm c}$ (ps)	$B(E2)e^2{\rm fm}^4$	$\lvert Q_t\rvert$ (eb)
89	$\frac{7}{2}^+$	10			>2.2 μs[d]		
132	$\frac{9}{2}^+$	43			<13 ns[d]	>105	
810	$\frac{11}{2}^+$	674			4.04(130)[d]	200(60)	
905	$\frac{13}{2}^+$	773			6.64(1.88)[d]	450^{180}_{100}	1.4^3_2
1866	$\frac{17}{2}^+$	961			1.44(43)[d]	690^{290}_{160}	1.6^3_2
1866	$\frac{17}{2}^+$	961	≥ 0.80	≥ 0.78	≥ 0.80	≤ 1245	≤ 2.1
2963	$\frac{21}{2}^+$	1097	0.34(7)	0.30(6)	0.32(7)	1610^{450}_{290}	2.3^3_2
3714	$(\frac{23}{2}^+)$	751	0.44(2)	0.68(23)	0.57(23)	400^{270}_{120}	
4107	$\frac{25}{2}^+$	1144	0.22(5)	0.28(6)	0.25(6)	1510^{470}_{290}	2.2^3_2
4752	$(\frac{27}{2}^+)$	646	0.38(8)	0.31(10)	0.35(10)	125^{50}_{30}	
4752	$(\frac{27}{2}^+)$	1039	0.28(6)	0.24(7)	0.26(7)	1010^{370}_{210}	1.8^3_2
5242	$(\frac{29}{2}^+)$	489		<0.50	<0.50		
5998	$(\frac{31}{2}^+)$	1246	<0.40	<0.36	<0.40	>680	>1.4
79	$\frac{5}{2}^-$	79			0.79(14) μs[d]		
366	$\frac{7}{2}^-$	287			77(22)[d]		
1911	$\frac{15}{2}^-$	856	≥ 1.1	≥ 1.7	≥ 1.7	<1050	<2.1
2448	$\frac{17}{2}^-$	943	0.8(2)	1.0(3)	0.86(30)	1270^{680}_{330}	2.2^5_3
2906	$(\frac{19}{2}^-)$	996	0.48(10)	0.59(15)	0.52(15)	1600^{650}_{360}	2.4^4_3
3495	$(\frac{21}{2}^-)$	1047	0.5(2)	0.6(2)	0.55(20)	1180^{670}_{710}	2.0^5_3
3980	$(\frac{23}{2}^-)$	1074	<0.6	<0.8	<0.8	>710	>1.5
4551	$(\frac{25}{2}^-)$	1056	<0.8	<0.7	<0.8	>780	>1.6
120	$\frac{1}{2}^{(+)}$	120			35(6) ns[d]		
221	$\frac{3}{2}^{(+)}$	221			0.91(29) ns[d]		
337	$\frac{5}{2}^{(+)}$	217			231(72)[d]	3960(1250)	4.5^{10}_6
558	$\frac{7}{2}^{(+)}$	337			≤ 25[d]	≥ 2700	≥ 3.2
1471	$\frac{13}{2}^{(+)}$	674		≥ 1.1	≥ 1.1	≤ 5300	≤ 4.1
1862	$\frac{15}{2}^{(+)}$	753		0.9(2)	0.9(2)	3750^{1070}_{680}	3.4^5_3
2326	$\frac{17}{2}^{(+)}$	855		0.44(12)	0.44(12)	4060^{1520}_{870}	3.5^6_4
2791	$\frac{19}{2}^{(+)}$	929		0.20(6)	0.20(6)	5900^{2530}_{1360}	4.2^8_5
3331	$\frac{21}{2}^{(+)}$	1005		0.24(7)	0.24(7)	3320^{1370}_{750}	3.1^6_4
3886	$\frac{23}{2}^{(+)}$	1095		0.19(6)	0.19(6)	2730^{1260}_{655}	2.8^6_4
4475	$(\frac{25}{2}^+)$	1144		0.13(4)	0.13(4)	3200^{1420}_{750}	3.1^6_4
5080	$(\frac{27}{2}^+)$	1194		<0.3	<0.3	>1120	>1.8
5753	$(\frac{29}{2}^+)$	1278		<0.1	<0.1	>2400	>2.6

[a]Lifetimes measured from the ^{28}Si + ^{56}Fe data.
[b]Lifetimes measured from the ^{29}Si + ^{55}Mn data.
[c]Adopted lifetime values.
[d]Reference 7.

The approximate degeneracy between the $[\tilde{2}\,\tilde{0}]$ levels in ^{81}Sr seen experimentally and calculated in Ref. 25 are consistent with conclusions of Ref. 29.

The lowest positive-parity state in ^{81}Sr is a $\frac{7}{2}^+$ level at an excitation energy of 89 keV. It is a member of a strongly decoupled $g_{9/2}$ rotational band. Theoretically[25] the $g_{9/2}$ single-neutron excitations with $K=\frac{5}{2}$ and $\frac{7}{2}$ correspond to the shapes with $\beta_2=-0.21$ and -0.18, respectively.

In addition to the near-oblate $g_{9/2}$ bandheads the Woods-Saxon calculations predict excited prolate $g_{9/2}$ orbitals $[422]\frac{5}{2}$ and $[413]\frac{7}{2}$ at $\beta_2=0.35$. They are expected to lie a few hundred keV above the ground state. In Ref. 7 the state at 203 keV has been tentatively assigned to $I^\pi=\frac{5}{2}^+$ based on the results of the beta-decay study[30] of ^{81}Y. A 203 keV level appears to be directly populated by the allowed beta transition with $\log(ft)=5.3$. Theoretically, the ground state of ^{81}Y is predicted to be the $[422]\frac{5}{2}$ state with a large quadrupole deformation. The $I^\pi=\frac{5}{2}^+$ ground state in ^{81}Y is also expected[30] experimentally from the systematics. The large moment of inertia of the ground-state rotational band in ^{81}Y suggests a considerable prolate deformation.[31] All these arguments indicate that the 203 keV level is the well-deformed $[422]\frac{5}{2}$ Nilsson orbital.

The $I^\pi=\frac{1}{2}^+$ bandhead seen[7] at 120 keV is most likely the $[431]\frac{1}{2}$ intruder state originating from the $d_{5/2}$ subshell. In the calculations this state also corresponds to a well-deformed prolate shape with $\beta_2=0.37$.

Summarizing this section, the deformed shell-model calculations give an interpretation of single-neutron excitations in ^{81}Sr in terms of the shape coexistence picture. Five observed bandheads can be interpreted as quasiparticle states coupled to the prolate core. On the other hand, the lowest $g_{9/2}$ excitations polarize the core towards oblate shapes. One may therefore expect strong shape-polarization effects associated with quasiparticle alignment to be present at high angular momenta. They are discussed in the following sections.

VI. ANGULAR MOMENTUM ALIGNMENT IN ^{81}Sr

The cranked shell model[32] (CSM) analysis of rotational bands in ^{81}Sr is presented in Figs. 10–13. Figure 10 shows the experimental Routhians versus rotational frequency for the positive-parity bands in ^{81}Sr, i.e., the $g_{9/2}$ band and the $d_{5/2}$ band. These bands are expected to have quite different shapes (see Sec. V). Therefore, it is rather meaningless to fit a common reference for the vacuum configuration. In order to present all the data on the same graph we have simply taken $J_0=11\hbar^2/\text{MeV}$, $J_1=0$ ("low" moment of inertia reference).

In the CSM analysis we assumed that the 3407 keV level is a $\frac{21}{2}^+$ state belonging to the one-quasi-particle $(1-qp)$ $g_{9/2}$ favored band with the signature quantum number $r=-i$. Indeed, when extrapolating the low spin part of the $r=-i$ $g_{9/2}$ Routhian to higher rotational frequencies, it approaches the $\frac{21}{2}^+$ (3407 keV) state (see Fig. 10).

The sequence built on the top of the $\frac{21}{2}^+$ yrast state at 2963 keV is a three-quasi-particle $(3-qp)$ configuration involving two aligned $g_{9/2}$ protons. It crosses the $g_{9/2}$ yrast band at $\hbar\omega_1=0.50$ MeV. At $\hbar\omega_2=0.56$ MeV an apparent second band crossing can be seen in the $r=-i$ band.

The signature splitting in the $1-qp$ $\pi=+$ band is large, characteristic of a decoupled configuration. Such a decoupled $g_{9/2}$ band has also been found in other $N=43$ isotones (see discussion in Refs. 3 and 7). On the other

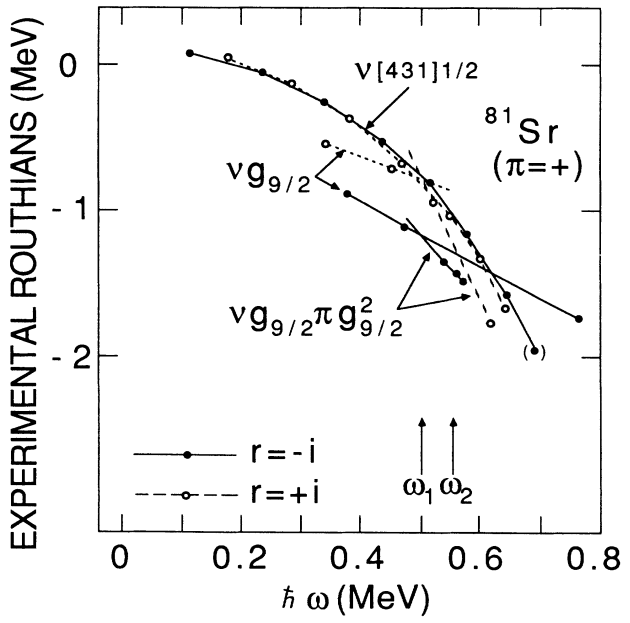

FIG. 10. Experimental Routhians for the positive-parity rotational bands in ^{81}Sr. The reference parameters are $J_0=11$ MeV/$\hbar^2$ and $J_1=0$ (see text).

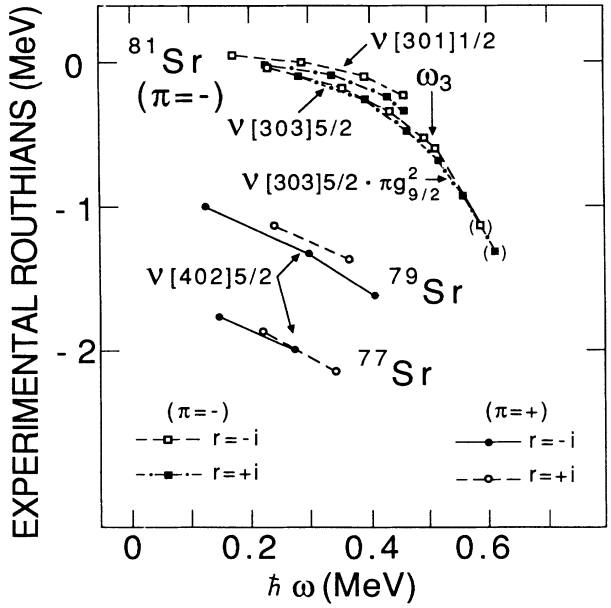

FIG. 11. Experimental Routhians for the negative-parity bands in ^{81}Sr and the $g_{9/2}$ bands (Ref. 4) in ^{77}Sr and ^{79}Sr. The latter ones have been artificially shifted down in energy in order to allow presentation on the same graph.

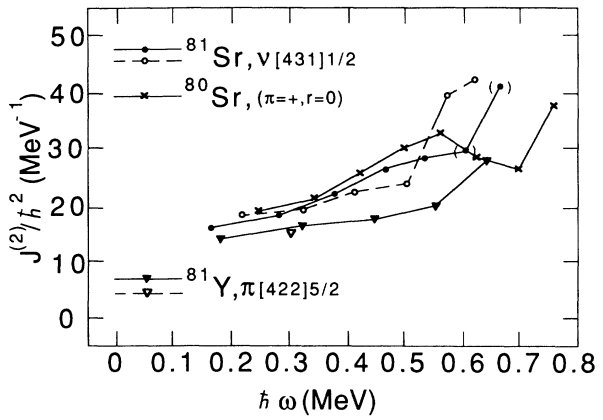

FIG. 12. Second moment of inertia for the $d_{5/2}$ band in ^{81}Sr, the yrast band (Ref. 5) in ^{80}Sr and the $g_{9/2}$ bands (Ref. 32) in ^{81}Y.

hand, in the $3-qp$ $\pi=+$ band the signature splitting significantly decreases. (Unfortunately, it is difficult to give a precise value for the signature splitting in this band. This is because both the $\frac{21}{2}^+$ and $\frac{29}{2}^+$ yrast states lie in the crossing regions and are disturbed by a band interaction.) Another interesting feature seen in the $3-qp$ band is strong $M1+E2$ ($\Delta I=1$) transitions. One can thus conclude that this band shows properties of a coupled configuration with a large $\langle K \rangle$ value.

A similar change in the rotational pattern in the $g_{9/2}$ band has previously been seen[33] in ^{81}Kr. Above $I^\pi=\frac{21}{2}^+$ a decoupled $g_{9/2}$ sequence is crossed by a coupled $3-qp$ band. Within the $3-qp$ band in ^{81}Kr the $\Delta I=1$ rates are so strong that the in-band $E2$ transitions have not been detected in Ref. 33.

The lighter Sr isotopes with $N=41$ and 39 are expected experimentally[4] and theoretically[25] to have very deformed prolate shapes. The $g_{9/2}$ [422]$\frac{5}{2}$ Routhians in ^{77}Sr and ^{79}Sr are displayed in Fig. 11. It can be observed that the signature splitting in the $1-qp$ $g_{9/2}$ band in the lighter Sr isotopes is considerably reduced compared to that in ^{81}Sr (at $\hbar\omega=0.35$ MeV it is almost zero in ^{77}Sr, about 120 keV in ^{79}Sr and about 300 keV in ^{81}Sr). This indicates a strong variation in the shape parameters of $g_{9/2}$ bands with neutron number. (If all three isotopes had similar prolate shapes the changes in the signature splitting would be exactly opposite to that observed experimentally.)

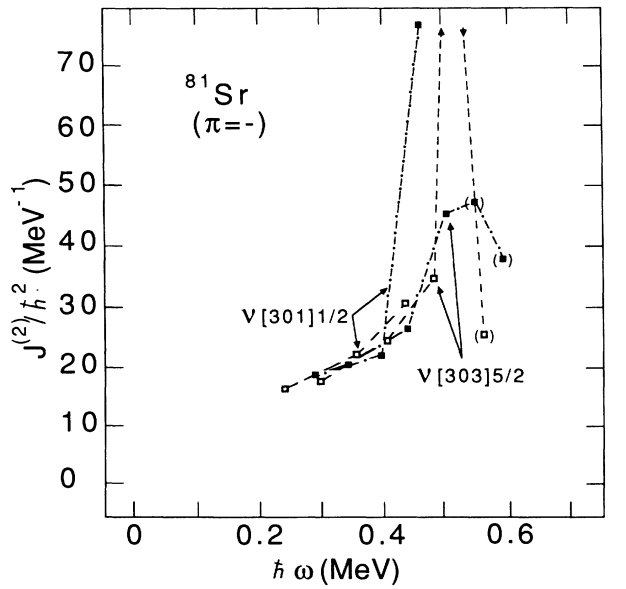

FIG. 13. Similar to Fig. 12 but for the $\pi=-$ bands in ^{81}Sr.

The $d_{5/2}$ band built on the [431]$\frac{1}{2}$ state does not show any strong irregularity up to highest spins observed. Due to its large moment of inertia it gradually approaches the $g_{9/2}$ bands but it never becomes yrast. The signature splitting between the $r=-i$ and $+i$ members of this band is very small. In order to magnify the fluctuations in the $d_{5/2}$ band its second (dynamical) moment of inertia, $J^{(2)}=dI/d\omega$, has been plotted in Fig. 12 together with the $J^{(2)}$ values for the yrast band in ^{80}Sr and the $g_{9/2}$ band in ^{81}Y. The $J^{(2)}$ moment of inertia for ^{80}Sr shows a smooth behavior with a maximum centered around $\hbar\omega=0.55$ MeV, which has been interpreted[25] as a gradual alignment of the $g_{9/2}$ proton pair. Above $\hbar\omega=0.7$ MeV a second upbending, associated with the alignment of the first neutron $g_{9/2}$ pair, starts to develop. The $r=-i$ member of the $d_{5/2}$ band has a very similar $J^{(2)}$ behavior. The hump in $J^{(2)}$ seen below $\hbar\omega=0.6$ MeV reflects, most likely, the $g_{9/2}$ proton crossing with a large band interaction. The irregularity seen at the last, tentative, data point may indicate the beginning of the neutron alignment. An increase in $J^{(2)}$ is more pronounced in the $r=i$ $d_{5/2}$ band. Its starts above $\hbar\omega=0.5$ MeV—which again is consistent with the alignment of a proton pair.

The experimental data for ^{81}Y fits to the proton crossing scenario. In the $g_{9/2}$ one-quasi-proton band the alignment of the first $g_{9/2}$ proton pair is blocked and indeed, neither irregularity nor hump in $J^{(2)}$ is seen around $\hbar\omega=0.55$ MeV there.

At low rotational frequencies both $\pi=-$ rotational bands built on the [301]$\frac{1}{2}$ and [303]$\frac{5}{2}$ Nilsson states have very similar rotational patterns (see Fig. 11). In both bands the signature splitting is very small, of the order of 50 keV. The $J^{(2)}$ moment of inertia in the $\pi=-$ bands in ^{81}Sr is shown in Fig. 13. At $\hbar\omega_3=0.51$ MeV the proton crossing is seen in both members of the [303]$\frac{5}{2}$ band and this value of proton crossing frequency is very close to the crossing frequency ω_1 in the $\pi=+$ sequence. In the $r=i$ [301]$\frac{1}{2}$ band the moment of inertia increases dramatically around $\hbar\omega=0.45$ MeV. Unfortunately, this band is known only up to $I=\frac{19}{2}$ which makes it difficult to conclude whether this irregularity is caused by a proton crossing or by some other structural changes.

VII. THEORETICAL ANALYSIS

A theoretical analysis of the rotational bands in ^{81}Sr has been performed using the Woods-Saxon cranking model of Ref. 25. Equilibrium shapes were calculated by minimizing the total Routhian with respect to deforma-

tion parameters β_2, β_4, and γ. As a residual interaction, the monopole pairing force has been taken with the strength from Ref. 25. At zero frequency self-consistent pairing gaps were calculated within the BCS model. At higher rotational frequencies, however, the pairing gaps were allowed to decrease gradually with increasing rotational frequency according to a simple analytical formula (for details see Refs. 3 and 34). The Fermi surfaces for protons and neutrons have been found numerically at each frequency from the particle number equation. The total Routhian in a fixed quasi-particle configuration (defined by means of parity, signature and excitation quantum numbers) was defined as a sum of the Strutinsky energy (liquid drop plus shell correction) and the rotational energy (calculated after solving the HFBC equations).

Figure 14 shows a few examples of total Routhian surfaces (TRS) for several quasi-particle configurations in ^{81}Sr calculated at different rotational frequencies. The upper portion of Fig. 14 corresponds to the positive-parity bands. At low rotational frequencies the $\pi=+$ TRS are very soft with respect to the (β_2,γ) parameters. The equilibrium deformation in the $g_{9/2}$ band has been calculated to be $\beta_2=0.23$, $\gamma=-50°$, corresponding to a near-oblate shape. The quasi-particle diagram representative for this configuration is shown in Fig. 15. The $g_{9/2}$ proton and neutron crossings are expected to occur at $\hbar\omega=0.5$ and 0.42 MeV, respectively. In both cases the band interaction is very small. Note the large signature splitting between the lowest $g_{9/2}$ Routhians.

At $Z=38$ the two-quasi-particle $g_{9/2}$ proton excitation drives the nuclear shape towards $\gamma=-30°$ (see Ref. 35) and indeed, in the $3-qp$ $\pi=+$ configuration the absolute minimum is moved to $\gamma=-30°$. Quasi-particle Routhians for $N=43$ at $B_2=0.22$, $\gamma=-33°$ are presented in Fig. 16 of Ref. 3. A neutron BC crossing is expected at $\hbar\omega=0.56$ MeV, in good agreement with experimental data. However, the signature splitting between the lowest $g_{9/2}$ neutron Routhians is still large at this triaxial shape, which might indicate that the calculations underestimate the range of the shape transition (a better agreement with experiment would be given by a larger value of γ, closer to the prolate axis; see Fig. 16).

A secondary near-prolate minimum with $\beta_2=0.33$ and $\gamma=-10°$ seen at $\hbar\omega=0.29$ MeV is representative for the $d_{5/2}$ band and the $g_{9/2}$ bands built on the $[413]\frac{7}{2}$ and $[422]\frac{5}{2}$ Nilsson states (see Fig. 18 of Ref. 3 for a neutron diagram). At this deformation the neutron $g_{9/2}$ signature splitting is very small and the neutron AB crossing with a very large band interaction is shifted to higher frequencies, $\hbar\omega>0.6$ MeV.

The lower portion of Fig. 14 shows TRS for $\pi=-$ configurations in ^{81}Sr. Before the proton alignment the

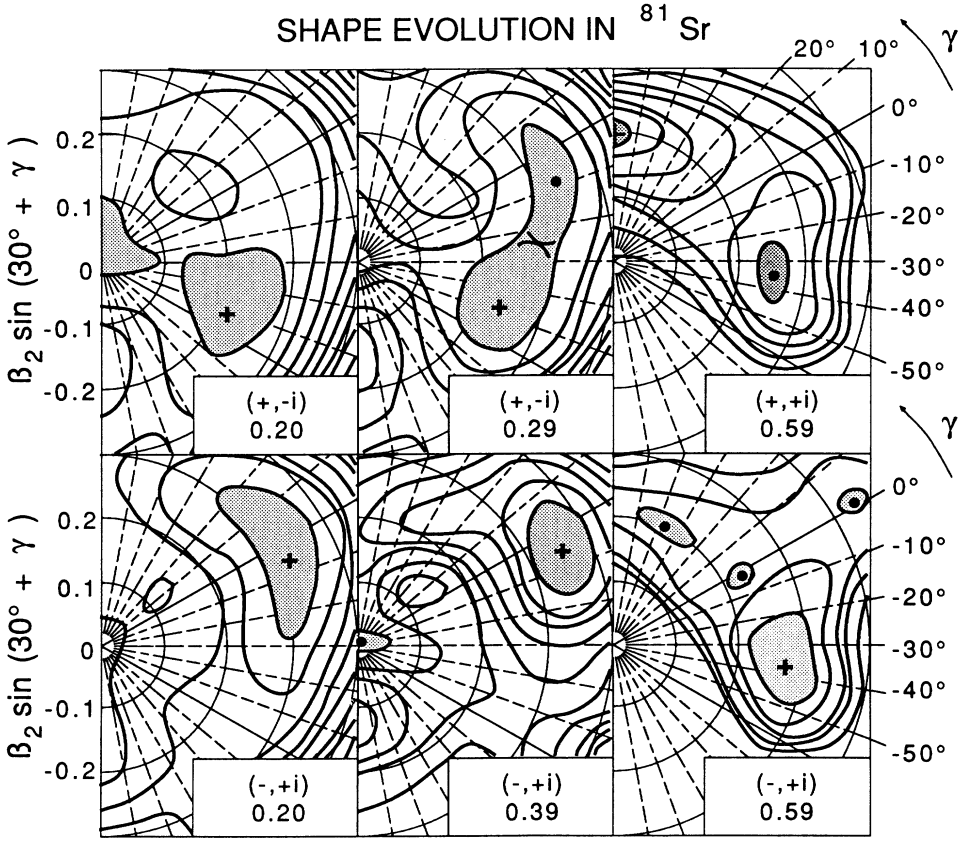

FIG. 14. Total Routhian surfaces (with pairing) in the (β_2,γ) plane for various quasi-particle configurations [labeled by means of the parity and signature (π,r) quantum numbers] in ^{81}Sr. The numbers give values of rotational frequency (in MeV). The distance between contour lines is 0.25 MeV.

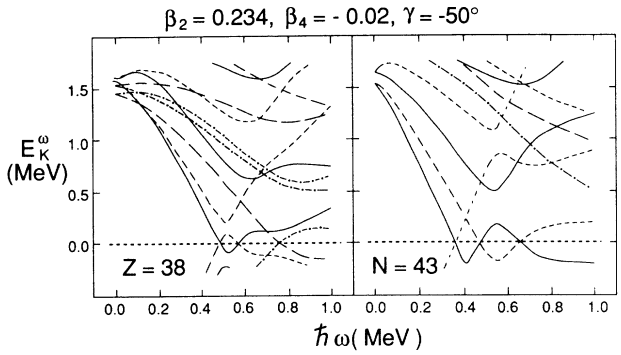

FIG. 15. Quasiparticle Routhians for ^{81}Sr at a deformation $\beta_2=0.234$, $\beta_4=-0.02$, $\gamma=-50°$, characteristic of the $g_{9/2}$ oblate bands. The spin and parity of the Routhians are indicated in the same way as in Figs. 10 and 11.

lowest negative-parity Routhians correspond to near-prolate shapes with $\beta_2=0.35$, $-10°\leq\gamma\leq-5°$. At this shape the signature splitting between the lowest $\pi=-$ Routhians is small (see Fig. 16). At $\gamma=-5°$ the $r=i$ excitation lies below the $r=-i$ Routhian (see below). However, when the γ parameter is decreased to about $-10°$ the signature order agrees with the experimental one (See Fig. 18 of Ref. 3). After alignment of a proton pair the γ deformation moves towards $\gamma=-30°$ (as in the $g_{9/2}$ band) and further alignment of $g_{9/2}$ neutrons shifts the equilibrium to even more negative γ values, $-50°\leq\gamma\leq-40°$.

Let us now discuss the lowest negative-parity Routhians in terms of the pseudo-SU(3) symmetry. For $N=43$ one can consider only three almost degenerate orbitals forming the $[\tilde{2}\,\tilde{0}]$ pseudo-oscillator subshell. In fact the $[\tilde{2}\,\tilde{1}]$ subshell consisting of the $[312]\frac{3}{2}$ and $[310]\frac{1}{2}$ orbitals is expected to influence significantly the rotational pattern only for lower particle numbers, around $N=36$. As in Ref. 36 we assume axial symmetry of the mean field. In such a case the orbital part of the Coriolis interaction, $\omega\tilde{I}_x$, does not introduce any rotational coupling. Therefore the Coriolis force acts only through the pseudospin part which, consequently, leads to the two groups consisting of three almost degenerate negative-parity Routhians with very small alignment (of the order of $\frac{1}{2}\hbar$). Experimentally (Fig. 11) and theoretically (Fig. 16) the lowest $\pi=-$ Routhians are indeed very similar and carry very little alignment before the first band crossing takes place. In the pseudospin limit the signature of the lowest quasiparticle state is expected to be $r=-i(-1)^{\tilde{N}}$ (see Ref. 27), i.e., $r=-i$ for $\tilde{N}=2$. Calculations at near-prolate shape indeed predict the $r=-i$ Routhian to be lower in energy. Experimental data, however, shows that the actual situation is reversed; the lowest $\pi=-$ one quasiparticle state has $r=+i$. As it was said above this apparent discrepancy can be explained by assuming negative γ deformation of about $-10°$.

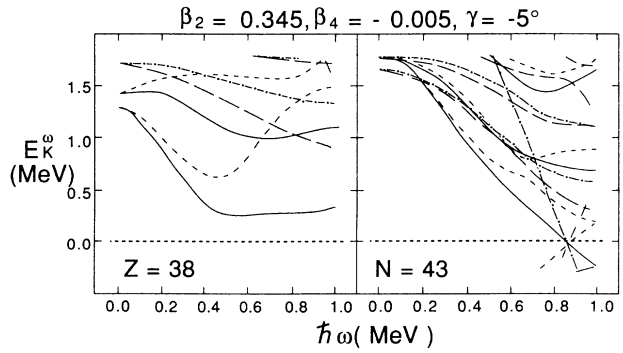

FIG. 16. Similar to Fig. 12, but at a deformation of $\beta_2=0.345$, $\beta_4=-0.005$, $\gamma=-5°$, characteristic of the near-prolate structures in ^{81}Sr.

The $[431]\frac{1}{2}$ band can be associated with the well-deformed prolate shape. At such a shape the proton alignment occurs very gradually because of the large band interaction at $Z=38$ (see Fig. 16 and the discussion of ^{80}Sr data in Ref. 25). This is consistent with a smooth increase in $J^{(2)}$ of the $d_{5/2}$ bands discussed in connection with Fig. 12.

The results of the lifetime measurements given in Table II are presented in Fig. 17 as a graph of Q_t versus $\hbar\omega$. As expected, the $g_{9/2}$ band shows very little collectivity at low spins. Its transition quadrupole moment is about 1.5 eb at $\hbar\omega\approx0.4$ MeV [which corresponds to quadrupole deformation of $\beta_2\approx0.19$ (cf. Sec. V)] and increases in magnitude, reaching a value of about 2.3 eb at $\hbar\omega\approx0.55$ MeV. This pattern can be qualitatively understood from Fig. 14. At low spins the $g_{9/2}$ band corresponds to an oblate shape with $\beta_2\approx0.20$ and a further reduction of the

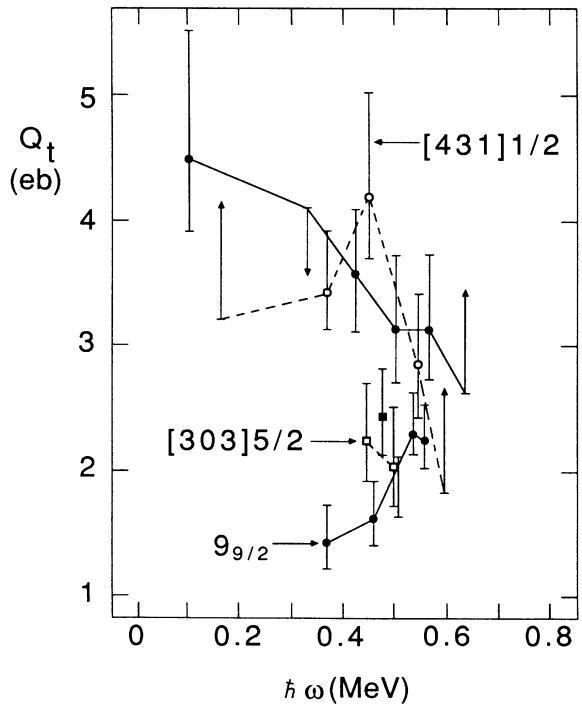

FIG. 17. Observed transition quadrupole moments Q_t [see Eq. (4)] in the $g_{9/2}$, $[431]\frac{1}{2}$, and $[303]\frac{5}{2}$ bands of ^{81}Sr, plotted as a function of rotational frequency. The states are marked in the same way as in Fig. 12.

quadrupole moment may be caused by an interaction with the low-lying spherical configuration. At higher frequencies, however, both β_2 and γ increase and, consequently, Q_t increases too.

One of the most interesting results of this study is the confirmation of the intruder nature of the $[431]\frac{1}{2}$ band. Its transition quadrupole moment is unusually large, about 3.5 eb, corresponding to an axial deformation of about 0.4. This agrees nicely with the results of the bandhead calculations discussed in Sec. V. At this point it has to be remarked that the results of the TRS calculations shown in Fig. 14 (top) do not allow us to separate the $d_{5/2}$ configuration in the (β_2,γ) plane, because at higher frequencies and larger deformations both the $d_{5/2}$ and $g_{9/2}$ orbitals carry the same quantum numbers and are mixed. The increase in $J^{(2)}$ at $\hbar\omega > 0.55$ MeV seen in the $[431]\frac{1}{2}$ band in Fig. 12 can be nicely correlated with the drop in Q_t seen in the same frequency interval. Due to the large value of proton band interaction the band crossing is very smooth and Q_t decreases gradually.

The transition quadrupole moments in the $[303]\frac{5}{2}$ band are around 2.2 eb; i.e., they are smaller than the theoretical predictions of Fig. 14 ($\beta_2=0.35$, i.e., $Q_t=3$ eb). One possible reason for this discrepancy would be the strong Coriolis mixing between the $[303]\frac{5}{2}$, $[301]\frac{3}{2}$, and $[301]\frac{1}{2}$ orbitals. However, this point still needs to be clarified.

Finally, we would like to comment on the results of the particle-rotor calculations of Ref. 7. In these calculations the single-particle orbitals were taken from the Nilsson model and an axially deformed prolate core with a quadrupole deformation of $\epsilon=0.3$ ($\beta_2=0.316$) was assumed. The particle-rotor approach gave a fair description of the $[303]\frac{5}{2}$ and $[431]\frac{1}{2}$ rotational bands. However, the calculations failed to reproduce the $[301]\frac{1}{2}$ and $g_{9/2}$ bands. For the $[301]\frac{1}{2}$ band the authors obtained a significant decoupling with the $r=i$ Routhian being yrast, in contrast to the experimental data. This discrepancy can be diminished by introducing a negative γ parameter (see discussion above). On the other hand, very small signature splitting and large $B(E2)$ values (around 100 W.u.) were predicted for the $g_{9/2}$ band. This large discrepancy can be immediately traced to the assumption of a well-deformed prolate shape used by the authors.

VIII. CONCLUSIONS

The present investigation has resulted in the placement of some 20 new γ rays and 15 new levels in the decay scheme of ^{81}Sr. The low spin level structure reported[7] by Arnell *et al.* was confirmed. The $g_{9/2}$ yrast band was studied up to spin $I^\pi=(\frac{31}{2}^+)$ and the onset of $3-qp$ excitations reported by Hicks *et al.*[9] was observed. However, the placement of levels near the vicinity of the $1-qp$ and $3-qp$ band crossing deduced in the present work was somewhat different than that previously reported.[9] The negative parity $K^\pi=\frac{5}{2}^-$ and $\frac{1}{2}^-$ bands were extended to spins of $I^\pi=(\frac{27}{2}^-)$ and $(\frac{19}{2}^-)$, respectively. Evidence of a $g_{9/2}$ proton alignment in the $K^\pi=\frac{5}{2}^-$ band was seen. The $K^\pi=\frac{1}{2}^{(+)}$ band was extended to spin $I^\pi=(\frac{31}{2}^+)$ and evidence of a gradual $g_{9/2}$ proton alignment was also seen.

The mean lifetimes of 12 states were measured and lifetime limits for 10 others were established using the Doppler-shift attenuation method. A consistency check for the analysis of the Doppler-shifted line shapes was provided through the use of data from two different reactions and target configurations. The $B(E2)$ values imply moderate deformations for both the $g_{9/2}$ and $K^\pi=\frac{5}{2}^-$ bands. In contrast, the $B(E2)$ values for transitions in the $K^\pi=\frac{1}{2}^{(+)}$ band indicate an average deformation nearly twice as large as that in the yrast band. These results are consistent with the results of lifetime measurements[7] by Arnell *et al.* for lower-lying states in the same bands.

The nuclei from the 70–80 mass region ($g_{9/2}$ region) have been known for many years to exhibit various signatures of shape coexistence. Among doubly-even nuclei the best examples are ^{70}Se and ^{72}Se, where an oblate ground state coexists with a well deformed prolate structure which becomes yrast at higher angular momenta (see, e.g., Ref. 36). In odd-A nuclei experimental information for coexisting oblate and prolate bands has been recently found[37] in ^{69}Se and ^{71}Se. All these nuclei belong to the lower half to the $g_{9/2}$ subshell.

^{81}Sr is probably the best known example of shape coexistence in the heavier nuclei from the $g_{9/2}$ region. The lowest $g_{9/2}$ neutron excitations in ^{81}Sr polarize the core towards oblate shapes, while prolate shapes are expected for the $\pi=-$ states and the $[431]\frac{1}{2}$ band.

A quite dramatic change in the positive-parity sequence has been observed after the first band crossing. It can be interpreted in terms of the shape change induced by the alignment of the $g_{9/2}$ proton pair which drives the equilibrium shape of the $3-qp$ $\pi=+$ configuration towards larger γ values. An analogous effect observed in ^{81}Kr has previously been given a similar explanation:[33] a transition from oblate to prolate shapes. The opposite tendency is expected for the lowest $\pi=-$ bands: after the alignment of proton and neutron quasiparticles the value of γ deformation decreases.

The intruder $d_{5/2}$ band shows signatures of a gradual $g_{9/2}$ proton alignment, characteristic of a well-deformed prolate shape. This is consistent with the very large values of transition quadrupole moment extracted from the experimental $B(E2)$ rates.

An interesting and not yet understood point is why the intensity in the unfavored $3-qp$ positive-parity yrast band is greater than that in the favored band. One possible explanation can be given in terms of the $g_{9/2}$ neutron crossing above $I=\frac{29}{2}$. Another possibility is the existence of noncollective isomeric states [seen in the $(+,+i)$ diagram of Fig. 14] which may influence the side feeding.

ACKNOWLEDGMENTS

The work of J. D. Fox, A. D. Frawley, E. G. Myers, L. Wright, P. Allen, and all the other persons involved in the construction of the Florida State University super-

conducting linac is gratefully acknowledged. This work was supported in part by the National Science Foundation. One of us (W.N.) was also supported by the Florida State University Supercomputer Computations Research Institute which is partially funded by the U.S. Department of Energy through Contract No. DE-FC05-85ER250000 and by the Polish Ministry of Science and Higher Education through Contract CPBP 01.09.

---

*Present address: Physics Division, Argonne National Laboratory, Argonne, IL 60439.

†Present address: Zweites Physikalisches Institut der Universität Göttingen, Bunsenstrasse 7-9, D-3400 Göttingen, Federal Republic of Germany.

‡Present address: Chemistry Department, Eastern Mennonite College, Harrisonburg, VA 22801.

§Present address: Department of Physics, University of Pennsylvania, Philadelphia, PA 19104.

[1]R. B. Piercey, J. H. Hamilton, R. Soundranayagam, A. V. Ramayya, C. F. Maguire, X. J. Sun, Z. Z. Zhoo, R. L. Robinson, H. J. Kim, S. Frauendorf, J. Döring, L. Funke, G. Winter, J. Roth, L. Cleeman, J. Eberth, W. Neumann, J. C. Wells, J. Lin, A. C. Rester, and H. K. Carter, Phys. Rev. Lett. **47**, 1514 (1981).

[2]J. H. Hamilton, P. G. Hansen, E. F. Zganjar, Rep. Prog. Phys. **48**, 631 (1985).

[3]U. J. Hüttmeier, C. J. Gross, D. M. Headly, E. F. Moore, S. L. Tabor, T. M. Cormier, P. M. Swertka, and W. Nazarewicz, Phys. Rev. C **37**, 118 (1988).

[4]C. J. Lister, B. J. Varley, H. G. Price, and J. W. Olness, Phys. Rev. Lett. **49**, 308 (1982).

[5]R. F. Davie, D. Sinclair, S. S. L. Ooi, N. Poofé, A. E. Smith, H. G. Price, C. J. Lister, B. J. Varley, and I. F. Wright, Nucl. Phys. **A463**, 683 (1987).

[6]P. S. Haskins, F. E. Dunham, R. L. Coldwell, A. C. Rester, R. B. Piercy, M. L. Muga, H. A. Van Rinsvelt, R. W. Smart, H. J. M. Aarts, J. D. Fox, L. C. Dennis, and C. B. Saw, Phys. Rev. C **32**, 1897 (1985).

[7]S. E. Arnell, C. Ekström, L. P. Ekström, A. Nilsson, I. Ragnarsson, P. J. Smith, and E. Wallander, J. Phys. G **9**, 1217 (1983).

[8]L. V. Theisen, S. L. Tabor, L. R. Medsker, G. Neuschaefer, L. H. Fry, Jr., and J. S. Clements, Phys. Rev. C **25**, 1325 (1982).

[9]G. C. Hicks, C. J. Gross, U. J. Hüttmeier, Xi-Ting Lu, G. Neuschaefer, and S. L. Tabor, Phys. Rev. C **29**, 1345 (1984).

[10]S. L. Tabor, Nucl. Instrum. Methods A **265**, 495 (1988).

[11]K. S. Krane, R. M. Steffen, and R. M. Wheeler, Nucl. Data Tables **11**, 354 (1973).

[12]P. Taras and B. Haas, Nucl. Instrum. Methods **123**, 73 (1975).

[13]L. C. Northcliffe and R. F. Schilling, Nucl. Data Sec. A **7**, 233 (1970).

[14]D. Ward, J. S. Forster, H. R. Andrews, I. U. Mitchell, G. C. Ball, W. G. Davies, and G. J. Costa, Atomic Energy of Canada Limited, Report AECL-5313, 1976.

[15]J. F. Ziegler and W. K. Chu, At. Data Nucl. Data Tables **13**, 463 (1974).

[16]S. Kalbitzer, H. Oetzmann, N. Grahmann, and A. Feverstein, Z. Phys. A **278**, 223 (1976).

[17]J. Lindhard, M. Scharff, and H. E. Schiøtt, Mat. Fys. Medd. Dan. Vid. Selsk. **33**, No. 14 (1963).

[18]A. E. Blaugrund, Nucl. Phys. **88**, 501 (1966).

[19]L. V. Theisen, L. R. Medsker, and S. L. Tabor, Phys. Rev. C **27**, 2679 (1983).

[20]A. Gavron, Phys. Rev. C **21**, 230 (1980).

[21]L. Funke, J. Döring, P. Kemnitz, E. Will, G. Winter, A. Johnson, L. Hildingsson, and Th. Lindblad, Nucl. Phys. **A455**, 206 (1986).

[22]J. Heese, K. P. Lieb, L. Lühmann, F. Raether, B. Wörmann, D. Albor, H. Grawe, J. Eberth, and T. Mylaeus, Z. Phys. A **325**, 45 (1986).

[23]L. Lühmann, M. Debray, K. P. Lieb, W. Nazarewicz, B. Wörmann, J. Eberth, and T. Heck, Phys. Rev. C **31**, 828 (1985).

[24]L. Lühman, K. P. Lieb, C. J. Lister, B. J. Varley, J. W. Olness, and H. G. Price, Europhys. Lett. **1**, 623 (1986).

[25]W. Nazarewicz, J. Dudek, R. Bengtsson, T. Bengtsson, and I. Ragnarsson, Nucl. Phys. **A345**, 397 (1985).

[26]A. Arima, M. Harvey, and K. Shimizu, Phys. Lett. **30B**, 517 (1969).

[27]A. Bohr, I. Hamamoto, and B. R. Mottelson, Phys. Scr. **26**, 267 (1982).

[28]K. T. Hecht and A. Adler, Nucl. Phys. **A137**, 129 (1969).

[29]J. Dudek, W. Nazarewicz, Z. Szymanski, and G. A. Leander, Phys. Rev. Lett. **59**, 1405 (1987).

[30]C. J. Lister, P. E. Haustein, D. E. Alburger, and J. W. Olness, Phys. Rev. C **24**, 260 (1981).

[31]C. J. Lister, R. Moscrop, B. J. Varley, H. G. Price, E. K. Warburton, J. W. Olness, and J. A. Becker, J. Phys. G **11**, 969 (1985).

[32]R. Bengtsson and S. Frauendorf, Nucl. Phys. **A327**, 139 (1979); **A314**, 27 (1979).

[33]L. Funke, F. Dönau, J. Döring, P. Kemnitz, E. Will, G. Winter, L. Hildingsson, A. Johnson, and Th. Lindblad, Phys. Lett. **120B**, 301 (1983).

[34]C. J. Gross, P. D. Cottle, D. M. Headly, U. J. Hüttmeier, E. F. Moore, S. L. Tabor, and W. Nazarewicz, Phys. Rev. C **36**, 2601 (1987).

[35]R. Bengtsson and W. Nazarewicz, Proceedings of the XIX Winter School, Zakopane, Poland, 1984, edited by Z. Stachura, Report IFJ No. 1268/PL, p. 171 (unpublished).

[36]J. H. Hamilton, *Heavy Ion Collisions,* Vol. 168 of *Lecture Notes in Physics* (Springer-Verlag, Berlin, 1982), p. 287.

[37]M. Wiosna, J. Busch, J. Eberth, M. Liebchen, T. Mylaeus, N. Schmal, R. Sefzig, S. Skoda, and W. Teichert, Phys. Lett. B **200**, 255 (1988).

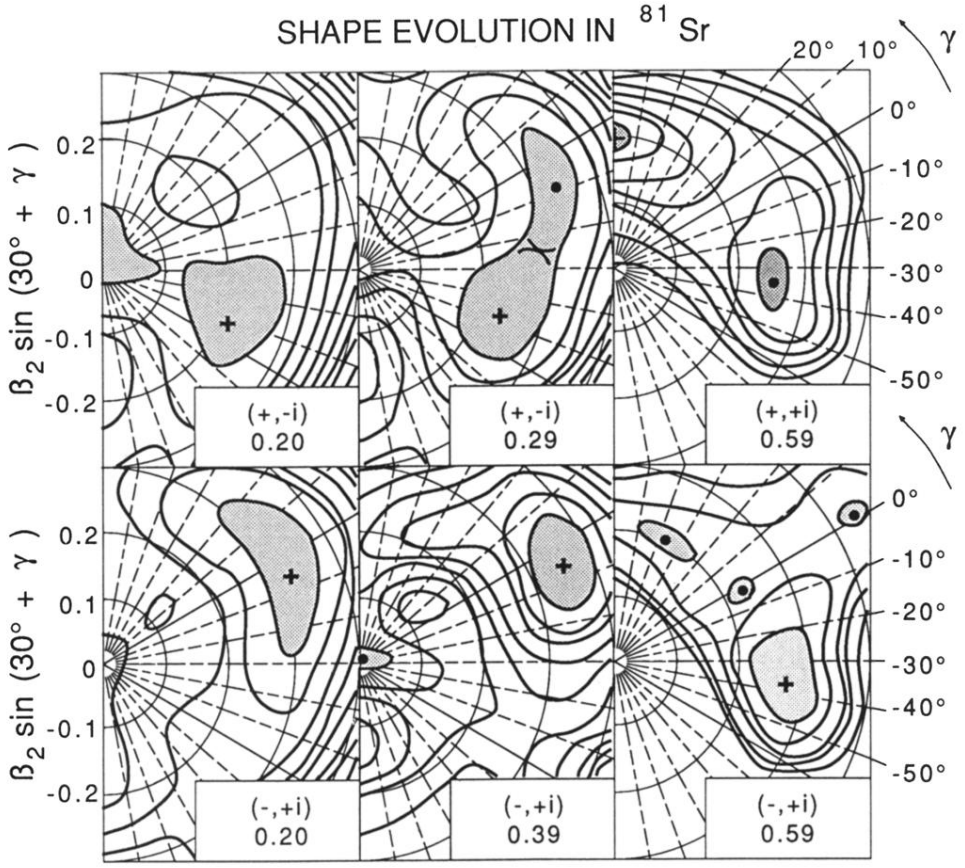

FIG. 14. Total Routhian surfaces (with pairing) in the (β_2,γ) plane for various quasi-particle configurations [labeled by means of the parity and signature (π,r) quantum numbers] in ^{81}Sr. The numbers give values of rotational frequency (in MeV). The distance between contour lines is 0.25 MeV.